Available online at www.sciencedirect.com
SCIENCE DIRECT®
Polymer 45 (2004) 3953–3959
polymer
www.elsevier.com/locate/polymer

# Structure-dynamics relationship in crystallizing poly(ethylene terephthalate) as revealed by time-resolved X-ray and dielectric methods

C. Alvarez[a,1], I. Šics[a,2], A. Nogales[a], Z. Denchev[a,3], S.S. Funari[b], T.A. Ezquerra[a,*]

[a]*Instituto de Estructura de la Materia, C.S.I.C. Serrano 119, Madrid 28006, Spain*
[b]*Max-Planck Intitute for Colloids and Surfaces, c/o HASYLAB, DESY, Notkestraße 85, 22603 Hamburg, Germany*

Received 17 May 2003; received in revised form 9 December 2003; accepted 9 December 2003

**Abstract**

The isothermal cold crystallization of poly(ethylene terephthalate) was investigated by simultaneous small and wide angle X-ray scattering (SAXS and WAXS) and dielectric spectroscopy (DS). By this experimental approach (SWD), simultaneously collected information was obtained about the specific changes occurring in both crystalline and amorphous phases during crystallization. The main features which are directly derived from our experiments can be explained assuming the formation of a heterogeneous multiple lamellar population arrangement. The rigid amorphous phase can be associated with the intra-lamellar stack amorphous phase. The restriction of the amorphous phase mobility mainly occurs in the inter-lamellar stacks regions probably due to the formation of secondary lamellae.


*Keywords:* Crystallization; Dielectric spectroscopy; Synchrotron radiation

## 1. Introduction

Poly(ethylene terephthalate) (PET) is one of the most common polymer provided by the polymer industry for fiber and packaging purposes [1,2]. As a consequence, research in PET has been approached from both technological and basic research sides. In particular, due to the fact that PET can be obtained either in the amorphous state or with a controlled amount of crystallinity, it has been frequently considered as a paradigm of semicrystalline polymers. Therefore, PET has been used to study the influence of crystallinity in a great variety of physical properties including thermal behavior [3–7], structure development [8–11] and mechanical and dielectric relaxational behavior [5,12–17] among others. Although crystallization of PET has been extensively investigated for many years there are several aspects that still remain controversial. On one hand, as far as the crystalline phase is concerned, X-ray scattering and transmission electronic microscopy (TEM) experiments probing the structure development upon crystallization were interpreted invoking the formation of a heterogeneous multiple lamellar population arrangement [9,18]. However, recent atomic force microscopy (AFM) studies seem to favor the formation of a more homogeneous lamellar space-filling structure [11]. On the other hand, in relation to the evolution of the amorphous phase dynamics during crystallization it was proposed, on the basis of thermal and dielectric analysis, the formation of a rigid amorphous phase located in the interfacial region between the crystalline lamellae and the inter-lamellar amorphous phase [5,15]. However, direct observation of the crystal-amorphous interphase in PET by means of AFM seems to indicate that the entire intra-lamellar amorphous phase should be considered as rigid [19]. Moreover, unexpectedly high oxygen solubility values of semicrystalline PET have been explained by assuming that the rigid amorphous phase is associated with the inter-lamellar amorphous phase [20]. From one experimental point of view, an improvement in the understanding of the correlation between microstructure and crystal development can be obtained by performing simultaneous small and wide angle x-ray scattering (SAXS and WAXS respectively) during isothermal crystallization

* Corresponding author.
*E-mail address:* imte155@iem.cfmac.csic.es (T.A. Ezquerra).
[1] Present address: Inst. de Ciencia y Tecnología de Polímeros CSIC, Juan de la Cierva 3, 28006 Madrid, Spain.
[2] Present address: Dept. of Chemistry, State University of New York, Stony Brook, NY 117943400.
[3] Present address: University of Minho, Department of Polymer Engineering, Guimarães-4800-038, Portugal.

0032-3861/$ - see front matter © 2004 Elsevier Ltd. All rights reserved.
doi:10.1016/j.polymer.2003.09.069

[21]. In addition, the information provided by SAXS and WAXS, about the structure of the ordered regions at different length scales, can be complemented simultaneously with that provided by dielectric spectroscopy (DS) about the amorphous phase [22]. Dielectric relaxation takes profit from the fact that, upon crystallization, polymer segmental dynamics is strongly affected by the progressive development of the crystalline phase [13,14,23].

In this paper we present real time isothermal crystallization experiments during cold crystallization of PET as revealed by means of simultaneous small-wide angle X-ray scattering and dielectric spectroscopy (SWD) measurements in real time. Provided that this procedure aims to obtain information from both the crystalline and the amorphous phase we attempt to shed additional light about the above discussed topics.

## 2. Experimental part

The material used in the present study was a commercial sample of PET (Rhodia S80 from RhodiaSter, $M_v = 45,000$ g/mol). Amorphous films of 0.2 mm thickness were produced by compression moulding of PET pellets at 300 °C for 3 min and subsequent quenching in ice water. Prior to the hot pressing, the original pellets were dried under vacuum for a given time to eliminate any existing traces of humidity that could cause hydrolysis during the preparation or investigation of the samples. Broad-band DS measurements of the complex dielectric permittivity ($\varepsilon^* = \varepsilon' - i\varepsilon''$), were performed from $10^{-1}$ to $10^6$ Hz by using a BDS-40 Novocontrol system and from $10^6$ to $10^9$ Hz by means of a Novocontrol BDS-60 coaxial line reflectometer. The temperature was controlled by means of a nitrogen gas jet (QUATRO from Novocontrol) with a temperature error of $\pm 0.1$ during every single sweep in frequency. Circular gold electrodes were sputtered onto the free surfaces of the films with a diameter of 3 cm for the measurements up to $10^6$ Hz and 0.5 cm for measurements at frequencies $F > 10^6$ Hz. Time-resolved SAXS-WAXS-DS experiments were performed in the Soft Condensed Matter beam-line A2 at HASYLAB in the synchrotron facility (DESY in Hamburg, Germany). To enable simultaneous measurements of small- and wide-angle X-ray scattering, as well as of DS in real time, an experimental cell (denominated as SWD) was employed [22]. The SWD cell was incorporated to a vacuum chamber ($10^{-2}$ Torr) specially designed to perform X-ray scattering measurements with synchrotron radiation. A wavelength $\lambda = 0.15$ nm was used for X-ray diffraction study. A semicrystalline PET standard sample was used for the WAXS and rat tendon tail for the SAXS calibration. Each frame was collected during 60 s and later corrected for primary beam intensity fluctuations during experiment and background. Complex dielectric permittivity measurements, ($\varepsilon^* = \varepsilon' - i\varepsilon''$) were performed in the frequency range of $10^0 \times$ Hz $< F < 10^5$ Hz, using a Novocontrol system integrating a SR 830 Lock-in amplifier with a BDC-L dielectric interface. Circular gold electrodes, 3 cm diameter, were employed to prepare a sandwich type capacitor.

## 3. Results

### 3.1. Dielectric relaxation of amorphous PET

Dielectric loss, $\varepsilon''$, and dielectric constant data, $\varepsilon'$, measured in the available frequency window at $T > T_g$ are shown as a function of frequency for different temperatures in Fig. 1. The broad-band data show not only the α-relaxation process, at lower frequencies, but also the subglass β-relaxation process at higher frequencies. As expected [14,24,25], the relaxations manifest themselves as maxima in $\varepsilon''$ and concurrent steps in $\varepsilon'$. As the temperature increases the frequencies of maximum loss, $F_{max}$, shift towards higher values. At low frequencies the relaxations are accompanied by a strong increase of $\varepsilon''$ corresponding to a dc-conductivity contribution. Isothermal $\varepsilon''$ and $\varepsilon'$ data can be phenomenologically described according to the Havriliak-Negami [14,26] equation given by:

$$\varepsilon^* = (\varepsilon_\infty)_\beta + \sum_{x=\alpha,\beta} \frac{(\varepsilon_0 - \varepsilon_\infty)_x}{[1 + (i\omega\tau_x)_x^b]_x^C} \quad (1)$$

Where $\varepsilon_0$ and $\varepsilon_\infty$ are the relaxed ($\omega = 0$) and unrelaxed ($\omega = \infty$) dielectric constant values, $\tau_x$ is the central relaxation time of the relaxation time distribution function, and $b$ and $c$ ($0 < b$, $c \leq 1$) are shape parameters which

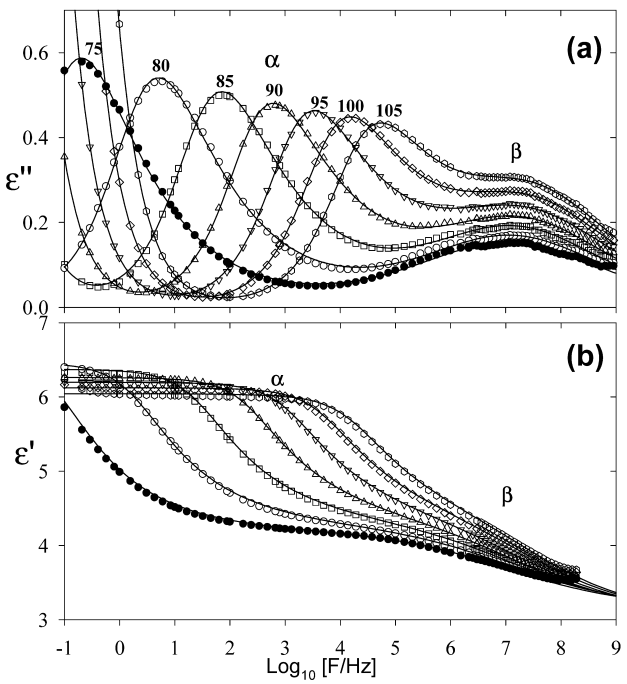


Fig. 1. (a) Amorphous PET dielectric loss, $\varepsilon''$, and (b) dielectric constant, $\varepsilon'$, values as a function of frequency for different temperatures labeled in °C.

describe respectively the symmetric and the asymmetric broadening of the relaxation time distribution function. The subscript makes reference either to the α or the β relaxation. The additional contribution of the conductivity process can be taken into account by adding a term: $-i\sigma/(\varepsilon_{vac}\omega^{s})$ to Eq. (1). Here $\sigma$ is related to the direct current electrical conductivity, $\varepsilon_{vac}$ is the dielectric constant of vacuum, and the value of the coefficient $0 < s < 1$ depends on the conduction mechanism [27]. The results from this phenomenological data analysis are shown in Fig. 1 by the continuous curves. The characteristic parameters of Eq. (1) are shown in Fig. 2(a) and (b) as a function of temperature. It is noteworthy that no parameter extrapolation from low temperature is needed while fitting the broad-band dielectric data of Fig. 1 due to experimental accessibility to both the α and the β relaxation in the same isotherm. Dielectric strength, $\Delta\varepsilon = \varepsilon_0 - \varepsilon_\infty$, values for the α-relaxation decrease strongly with temperature while the corresponding ones for the β-relaxation tend to increase. Amorphous PET presents an strongly asymmetric α-relaxation as denoted by an asymmetric broadening parameter $c = 0.4$ nearly constant in the studied temperature range. On the contrary the β-relaxation is symmetric, $c = 1$, in the presented temperature range. The central relaxation time, $\tau$, has been represented in Fig. 2(b) as a function of the reciprocal temperature for both relaxations. In such a representation, the β relaxations follow an Arrhenius behavior characteristic of a non-cooperative process [14,24]. The activation energy associated to this process is about 13 kcal/mol. The origin of the β subglass relaxation has been traditionally associated to the local motion of the ester group [14,24]. Recent dielectric measurements of the β-relaxation in PET indicated a more complex molecular origin [28]. Here, Bravard and Boyd propose that the β-process may consist of the contribution of three types of bonds namely: (a) the aromatic ring carbon to ester carbon, (b) the ester ether oxygen to aliphatic carbon and (c) the aliphatic carbon–carbon bond. This hypothesis is supported, on one hand, by the dielectric measurements at low temperature which reveal the existence of several components in the β-relaxation dielectric spectrum [28] and, on the other hand, by molecular dynamics simulation [29,30]. In the temperature range covered in Fig. 1, the β-relaxation can be well described as a single Cole–Cole process (HN-equation with $c = 1$). This is expected because extrapolation of the results from Bravard and Boyd show that the three contributions of the β-relaxation tend to coalesce at temperatures higher than ≈60 °C. In the case of the α-relaxation, which appears as a consequence of the segmental motions of the amorphous phase above the glass transition temperature, the dependence of $\log_{10}[\tau]$ with the reciprocal temperature exhibit a certain curvature which can be described by means of the Vogel–Fulcher–Tamann (VFT) equation:

$$\log_{10}[\tau] = A + B/(T - T_0) \quad (2)$$

The VFT parameters in this case are, $A = -11$, $B = 448\ K$ and $T_0 = 310$ K in agreement with previous measurements [28].

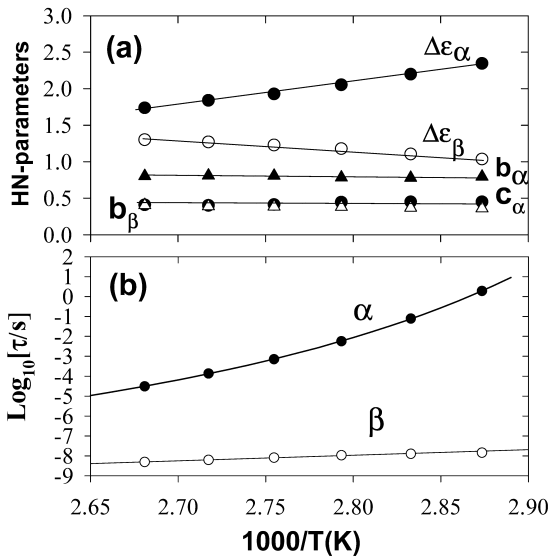


Fig. 2. Results of the fittings of the dielectric data for amorphous PET to the HN equation. (a) (●) $\Delta\varepsilon_\alpha$. and (○) $\Delta\varepsilon_\beta$ are the dielectric strength of the α and β-relaxation respectively; (▲) $b_\alpha$ and (△) $b_\beta$ are the broadening parameter for α and β relaxation respectively and (●) $c_\alpha$ is the asymmetry parameter for the α-relaxation, $c_\beta = 1$. (b) Central relaxation times (●) $\tau_\alpha$ and (○) $\tau_\beta$ for the α and β relaxation, respectively.

### 3.2. Time resolved cold crystallization of PET

Fig. 3 shows the time-resolved SAXS-WAXS-DS data simultaneously collected during a cold crystallization experiment at $T_c = 96$ °C for three different crystallization times covering the crystallization process. Both, WAXS and Lorentz corrected SAXS intensities [31] are given as a function of the scattering vector $s = (2/\lambda)\sin\theta$, $2\theta$ being the scattering angle. The $\varepsilon''$ data from DS are presented as a function of frequency. The initial amorphous state is characterized by a broad halo in the WAXS diagram, by a continuous scattering in the SAXS pattern, which is due to the liquid-like state, and by the presence of a relaxation process characterized as a maximum in $\varepsilon''$ centered around a $F_{max}$ value of $4 \times 10^3$ Hz in the DS data. The observed relaxation can be identified with the α-process. As time increases, the onset of crystallization is manifested by the incipient appearance of Bragg peaks in the WAXS patterns characterizing respectively the (010), (1 − 10) and (100) reflections of the triclinic unit cell of PET. The weight fraction index of crystallinity ($X_c$) can be estimated from the ratio between the area below the crystalline Bragg peaks to the total scattered area after appropriate subtraction of a flat background [32]. Dashed lines in Fig. 3 show the peak deconvolution procedure. In the SAXS patterns an increase of the scattered intensity at lower $s$-values that develops into a well defined peak centered around a value of $s = 0.125$ $nm^{-1}$ is observed. This fact indicate that lamellar crystals

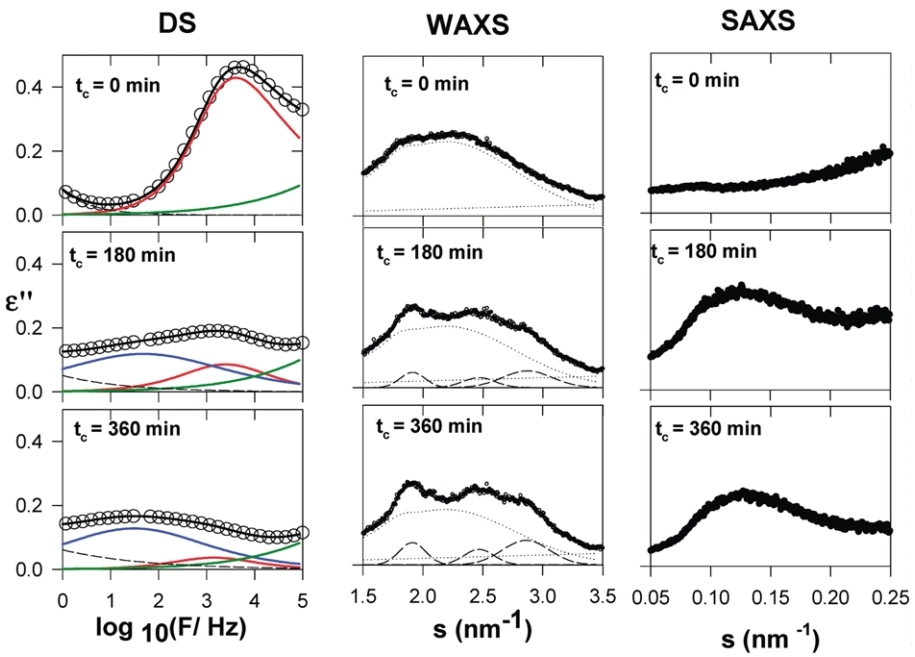


Fig. 3. Simultaneous dielectric loss, $\varepsilon''$, WAXS and, SAXS experiments during crystallization of initially amorphous PET at $T_c = 96°$ C for three different crystallization time covering the crystallization process. Continuous lines in the DS-data indicate the separate contribution of the primary and secondary α-relaxations, the β-relaxation tail appearing at higher frequencies and the conductivity tail appearing at lower frequencies. Dotted and dashed lines in the WAXS-data illustrate the peak deconvolution procedure.

organize themselves forming a nanostructure of lamellar stacks with an average distance between gravity centers of consecutive lamellar crystals of $L = 1/s_{max} \approx 8$ nm. The above mentioned structural features are accompanied by changes in the dynamics of the amorphous phase as revealed by the simultaneous DS experiment. The α-relaxation exhibits, at the end of crystallization a decrease in its intensity and a shift towards lower values of $F_{max}$. At intermediate crystallization times a significant broadening in the low frequency side of the relaxation is detected. This effect, previously reported by Fukao et al. [33], can be described as an additional α-process, α′, appearing as crystallinity develops. The dielectric data were analyzed in terms of the HN-equation considering the contribution of (i) the initial α-process; (ii) the second α-process appearing during crystallization (iii) the β-relaxation process which contributes in the higher frequency range of the spectrum and (iv) the conductivity which influences the lower frequency part of the spectrum. In this case the NH-equation used for the fittings reads:

$$\varepsilon^* = \varepsilon_\infty + \frac{(\Delta\varepsilon)_\alpha}{[1+(i\omega\tau_\alpha)^{b_\alpha}]^{c_\alpha}} + \frac{(\Delta\varepsilon)_{\alpha'}}{[1+(i\omega\tau_{\alpha'})^{b_{\alpha'}}]^{c_{\alpha'}}} + \frac{(\Delta\varepsilon)_\beta}{[1+(i\omega\tau_\beta)^{b_\beta}]^{c_\beta}} - i\frac{\sigma}{\varepsilon_{vac}\omega^s} \quad (3)$$

The separate contribution of every process as well as the total fittings are shown in Fig. 3 by the continuous lines. The initial parameters to simulate the β-relaxation where taken considering the broad-band data of Fig. 2. A visualization of the changes in the characteristic parameters simultaneously measured is presented in Fig. 4. In this figure we have represented as a function of the crystallization time for both the initial and the secondary α′-relaxation process: (a) the dielectric strength, (b) the broadening parameter (c) the asymmetry parameter (d) the central relaxation time. Additionally values for the weight fraction index of crystallinity ($X_c$) are included (Fig. 4(e)) calculated from the WAXS data.

## 4. Discussion

From the simultaneous SWD-experiments a relationship between structure and dynamics can be attempted. For times shorter than a characteristic one in our case $t \approx 90$ min. at $T = 96$ °C, the initial strong reduction of the mobile material, reflected by the decrease of $\Delta\varepsilon_\alpha$ (Fig. 4(a)), parallels the increase of crystallinity (Fig. 4(e)). However, as observed in a great amount of polymers [13,34], the reduction of the mobile material characterized by the decrease of $\Delta\varepsilon_\alpha$ is stronger than the increment in crystallized material as determined by the increase of $X_c$. This effect can be attributed to the formation of an immobilized amorphous phase frequently referred to as rigid amorphous phase (RAP) [35]. During this initial period of crystallization, in spite of the strong reduction in $\Delta\varepsilon_\alpha$ of about 50%, the remaining mobile material only slightly change the average segmental mobility in the amorphous phase as reflected by the moderate variation observed in $\tau_\alpha$ (Fig. 4(d)). During this initial period the relaxation tends to

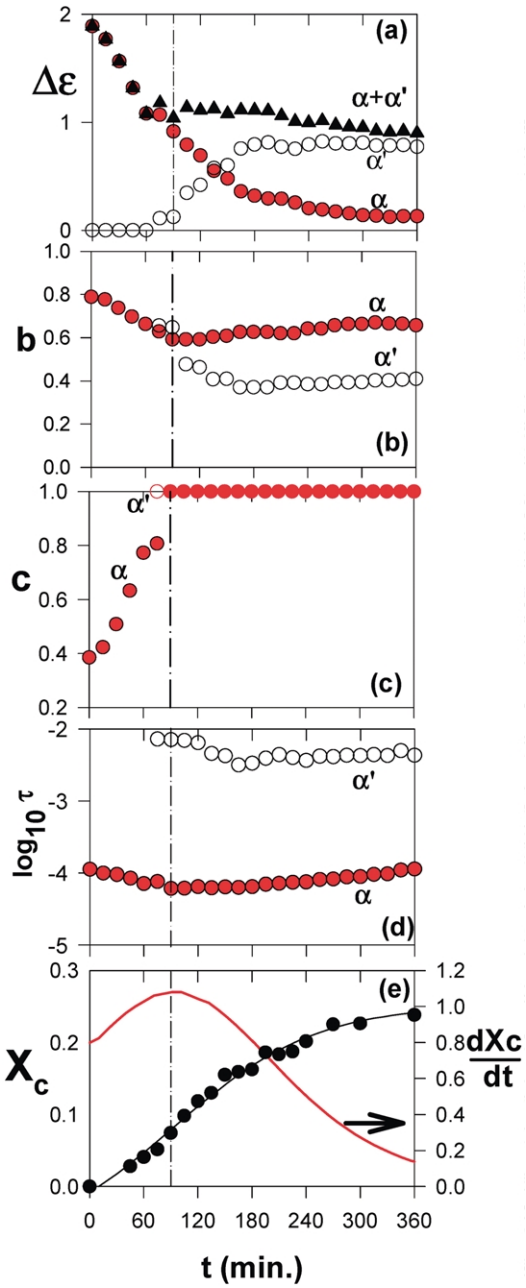


Fig. 4. Summary of physical parameters obtained from the SWD experiment for PET at $T = 96°C$ as a function of the crystallization time: (a) (●) $\Delta\varepsilon$ values for the α-relaxation, (○) α′-relaxation and (▲) $\Delta\varepsilon_\alpha + \Delta\varepsilon_{\alpha'}$. (b) Broadening parameter for the (●) α-relaxation and (○) α′-relaxation. (c) Asymmetry parameter for the (●) α-relaxation and (○) α′-relaxation. (d) Central relaxation times for the (●) α-relaxation, (○) α′-relaxation. (e) Crystallinity index (left) and slope of the crystallinity curve (right).

become symmetric and increasingly broader, as denoted by the increase of the $c_\alpha$-parameter and the decrease of the $b_\alpha$-parameter respectively (Fig. 4(b) and (c)). As crystallization proceeds above the characteristic time, a secondary α-relaxation, α′, is detectable as a low frequency shoulder in the $\varepsilon''$ measurements (Fig. 3). The maximum of the α′-relaxation appears at significant lower frequencies, i.e. higher values of $\tau_{\alpha'}$, as those compared with the initial α-relaxation. The fittings indicate that the α′-relaxation can be described as a symmetric process ($c_{\alpha'} = 1$). As crystallization time increases the dielectric strength of the α′-relaxation, $\Delta\varepsilon_{\alpha'}$, tends to increase at expenses of $\Delta\varepsilon_\alpha$. (Fig. 4(a)) as revealed by the moderate variation of the magnitude defined by $\Delta\varepsilon_\alpha + \Delta\varepsilon_{\alpha'}$ (triangles in Fig. 4(a)). At the end of the crystallization process $\Delta\varepsilon_\alpha$ tends to zero and the secondary process becomes the characteristic α-relaxation of the semi-crystalline material.

The above features, which emerge directly from the simultaneous SAXS, WAXS and DS experiments enable us to propose the following explanation for the cold crystallization of PET. During the initial stages of the process, before the characteristic time, lamellar crystals develop involving a strong formation of rigid amorphous phase as revealed by the increase observed in $X_c$ and the decrease of $\Delta\varepsilon_\alpha$. In this regime the average mobility of the remaining mobile amorphous phase is slightly affected, as revealed by the small variation with time of $\tau_\alpha$. We propose that the amorphous regions located between consecutive crystals within the lamellar stack become immobilized as soon as the lamellar stack is formed during the initial stages of crystallization before the characteristic time. This could explain the strong reduction of $\Delta\varepsilon_\alpha$ for moderate increase of $X_c$. A similar model was recently proposed to explain oxygen transport properties of PET [20]. In fact, oxygen permeation measurements indicate that the amorphous region within the lamellar stacks can be associated with the rigid amorphous phase (RAP) [18]. Moreover, recent AFM observations of the inter-lamellar amorphous phase PET indicate that molecular mobility in these regions should be strongly inhibited [19]. Accordingly, in this initial stage, the α-relaxation could predominantly originate in the inter-lamellar stacks amorphous regions. Around the characteristic time a significantly slower process appears, the α′-relaxation. Experiments performed in PET at higher temperatures [36] indicate that the transition from the primary to the secondary α-relaxation process occurs upon passing from the initial to the final crystallization regimes. The separation between primary and secondary crystallization has been associated with the moment in which spherulite impingement occurs [37]. After impingement, crystallization can proceed by formation of secondary crystals additionally to the growth of the initial primary crystals. In fast crystallization experiments for PET the transition from primary to secondary crystallization is rather well defined [21,36]. Due to the fact that in the present case cold crystallization takes place relatively close to $T_g$ the process the crystallinity evolution spreads in time. Thus, the transition from primary to secondary crystallization regimes is not so well defined as for crystallizations at higher temperatures. By calculating the slope of $X_c$ with time, continuous line referred to the right y-axis, in Fig. 4(e), it is observed that the characteristic time at which the secondary α-relaxation starts to appear is close to the inflexion point of

the crystallinity curve. This inflexion point can be associated to the moment in which significant impingement of lamellar stacks may locally occur during primary crystallization. After impingement secondary crystals are likely to develop. This suggests that secondary crystals growing in the inter-lamellar stacks amorphous phase may act as physical cross-links tending to slow-down segmental dynamics and giving rise to the secondary α-relaxation. A simplistic scheme of the proposed model is described in Fig. 5. Here Fig. 5(a) represents the initial amorphous state in which only the primary α-relaxation is present. Fig. 5(b) represent the primary lamellar stacks. Here, the segmental mobility of the intra-lamellar stack amorphous phase is arrested and the α-relaxation mainly originates in the inter-lamellar stacks amorphous regions. Thus the overall segmental mobility is essentially similar to the initial one. Fig. 5(c) represents the moment in which secondary crystals start growing in the inter-lamellar stacks amorphous regions. Here it exists a coexistence of the primary α-process, occurring in the inter-lamellar stacks amorphous regions free of secondary lamellae, and of the secondary α-relaxation taking place in the inter-lamellar stacks amorphous regions in which secondary lamellae start to grow. A qualitatively similar model was recently proposed to explain cold crystallization experiments in poly(ether ether ketone)(PEEK) [37] and poly(ethylene naphthalene-2,6-dicarboxylate)(PEN) [38]. Similar results for PET have been previously discussed by Fukao et al. [33]. These authors explained the appearance of the secondary α-process as being characteristic of a coexistence state somehow precursor of the crystalline state. The analysis of our time resolved SWD experiments for PET indicate that also an explanation based on the structural heterogeneity of PET can support the experiments findings without precluding the existence of such a coexistence state in the amorphous phase.

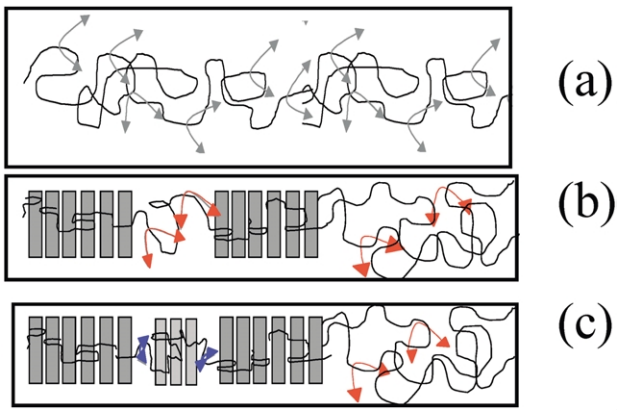


Fig. 5. Schematic model for the cold crystallization of PET. (a) Before crystallization polymer chains present segmental motion (schematically depicted by the curved arrows) leading to the α-relaxation. (b) During the growing of the primary lamellar stacks (sets of gray bars) the segmental mobility of the intra-lamellar stack amorphous phase is arrested and the α-relaxation mainly originates in the inter-lamellar stacks amorphous regions. (c) Secondary lamellae grow in the inter-lamellar stacks amorphous regions. The primary α-process, occurring in the inter-lamellar stacks amorphous regions free of secondary lamellae coexists with the secondary α′-relaxation taking place in the inter-lamellar stacks amorphous regions in which secondary lamellae start to grow.

## 5. Conclusions

In summary, the main features which are directly derived from our simultaneous SAXS, WAXS and DS experiments for the cold crystallization of PET can be explained assuming the formation of a heterogeneous multiple lamellar population arrangement. The rigid amorphous phase can be associated with the intra-lamellar stack amorphous phase. The restriction of the amorphous phase mobility mainly occurs in the inter-lamellar stacks regions probably due to the formation of secondary lamellae.

## Acknowledgements

The authors are indebted to MCYT (grant FPA2001-2139) Spain, for generous support of this investigation. The experiments at HASYLAB(Hamburg, Germany) have been funded by the IHP-Contract HPRI-CT-1999-00040 of the European Commission (EC(ERBFMGEDT 950059) and II-00-015 EC). C.A. thanks the Comunidad de Madrid (Spain) for the tenure of a post-doctoral fellowship.

## References

[1] Paul DR, Barlow JW, Keskkula H. In: Mark HF, Bikales NM, Overberger ChG, Menges G, editors. Encyclopedia of polymer science and engineering, vol. 12. New York: Wiley; 1989.
[2] Fakirov S, editor. Handbook of thermoplastic polyesters. Weinheim: Wiley-VCH; 2002.
[3] Groeninckx G, Reynaers H, Berghmans H, Smets G. J Polym Sci Polym Phys 1980;18:3111.
[4] Monserrat S, Cortés P. J Mater Sci 1995;30:1790.
[5] Dobbertin J, Hensel A, Schick C. J Thermal Anal 1996;47:1027.
[6] Medellin-Rodriguez FJ, Phillips PJ, Lin JS. Macromolecules 1996;29:7491.
[7] Alves NM, Mano JF, Balaguer E, Dueñas JMM, Ribelles JLG. Macromolecules 2002;43:4111.
[8] Jonas AM, Russell TP, Yoon DY. Colloid Polym Sci 1994;272:1344.
[9] Santa Cruz C, Stribeck N, Zachmann HG, Baltá-Calleja FJ. Macromolecules 1991;24:5980.
[10] Wang ZG, Hsiao BS, Fu BX, Liu L, Yeh F, Sauer BB, Chang H, Schultz JM. Polymer 2000;41:1791.
[11] Ivanov DA, Amalou Z, Magonov SN. Macromolecules 2001;34:8944.
[12] Schermann W, Zachmann HG, Kolloid-Z.u Z. Polymere 1970;241:921.
[13] Williams G. Adv Polym Sci 1979;33:59.
[14] Coburn JC, Boyd RH. Macromolecules 1986;19:2238.
[15] Schick C, Donth E. Phys Scr 1991;43:423.
[16] Vigier G, Tatibouet J, Benatmame A, Vassoille R. Colloid Polym Sci 1992;270:1182.

[17] Ezquerra TA, Baltá-Calleja FJ, Zachmann HG. Polymer 1994;35:2600.
[18] Xia Z, Sue H, Wang Z, Avila-Orta CA, Hsiao BS. J Macromol Sci Phys 2001;B40:625.
[19] Ivanov DA, Pop T, Yoon DY, Jonas AM. Macromolecules 2002;35:9813.
[20] Lin J, Shenogin S, Nazarenko S. Polymer 2002;43:4733.
[21] Zachmann HG, Wutz C. In: Dosiëre M, editor. Crystallization of polymers. Amsterdam: Kluwer Academic Publishers; 1993.
[22] Šics I, Nogales A, Ezquerra TA, Denchev Z, Baltá-Calleja FJ, Meyer A, Döhrmann R. Rev Sci Instrum 2000;71:1733.
[23] Ezquerra TA, Majszczyk J, Baltá-Calleja FJ, López-Cabarcos E, Gardner KH, Hsiao BS. Phys Rev B 1994;50:6023.
[24] McCrum NG, Read BE, Williams G. Anelastic and dielectric effects in polymeric solids. New York: Dover; 1991.
[25] Hofmann A, Kremer F, Fischer EW. Physica A 1993;201:106.
[26] Havriliak S, Negami S. Polymer 1967;8:161.
[27] Kirst KU, Kremer F, Litinov VM. Macromolecules 1993;26:975.
[28] Bravard SP, Boyd RH. Macromolecules 2003;36:741.
[29] Hedenqvist M, Bharadwaj R, Boyd RH. Macromolecules 1998;31:1556.
[30] Boyd SU, Boyd RH. Macromolecules 2001;34:7219.
[31] Baltá-Calleja FJ, Vonk CG. X-ray scattering of synthetic polymers. Amsterdam: Elsevier; 1989.
[32] Blundell DJ, Osborn BN. Polymer 1983;24:953.
[33] Fukao K, Miyamoto Y. Phys Rev Lett 1997;79:4613.
[34] Ezquerra TA, Nogales A. In: Sommer JU, Reiter G, editors. Polymer crystallization: observations, concepts and interpretations, lecture notes in physics, 606. Heidelberg: Springer; 2003.
[35] Cheng SZD, Wu ZQ, Wunderlich B. Macromolecules 1987;20:2802.
[36] Ezquerra TA, Šics I, Nogales A, Denchev Z, Baltá-Calleja F. J Europhys Lett 2002;59:417.
[37] Nogales A, Ezquerra TA, Denchev Z, Šics I, Baltá-Calleja FJ, Hsiao B. J Chem Phys 2001;115:3804.
[38] Šics I, Ezquerra TA, Nogales A, Denchev Z, Alvarez C, Funari SS. Polymer 2003;44:1045.